IDA

INSTITUTE FOR DEFENSE ANALYSES

Visible Signatures of Hypersonic Reentry

Jeremy Teichman
Leon Hirsch

February 2013
Approved for public release;
distribution is unlimited.
IDA Document NS D-4792
Log: H 13-000192

INSTITUTE FOR DEFENSE ANALYSES
4850 Mark Center Drive
Alexandria, Virginia 22311-1882

The Institute for Defense Analyses is a non-profit corporation that operates three federally funded research and development centers to provide objective analyses of national security issues, particularly those requiring scientific and technical expertise, and conduct related research on other national challenges.

About This Publication
This work was conducted under IDA's independent research program (C2165). The views, opinions, and findings should not be construed as representing the official position of either the Department of Defense.

INSTITUTE FOR DEFENSE ANALYSES

IDA Document NS D-4792

Visible Signatures of Hypersonic Reentry

Jeremy Teichman
Leon Hirsch

Visible Signatures of Hypersonic Reentry

J. Teichman[1] and L. Hirsch[2]
Institute for Defense Analyses, Alexandria, VA 22311

Aerothermal heating of hypersonic reentry bodies can generate significant radiation of visible light. Here, we investigate the conditions for ground-level visibility and what we term *noticeability* of that radiated light to the unaided human eye. We consider radiated visible light, transmission to ground level as a function of relative observer position, sky background contrast, human contrast perception limits, and psychophysical considerations for attention capture. Considering both pure ballistic trajectories and lifting-body trajectories, we show some examples where we calculate the spatial and temporal viewing zones for both detectability and noticeability. In some cases, these viewing zones extend a significant distance from the impact location and/or include the impact location for a potentially significant period of time before impact.

Nomenclature

V = reentry body velocity [m/s]

ρ = ambient air density [kg/m^3]

ρ_0 = sea-level air density [kg/m^3]

φ = luminous power [lumens]

J_s = volumetric luminous intensity at stagnation point [candelas/m^3]

R_N = radius of curvature of reentry body nose [m]

T = stagnation temperature [K]

T_∞ = ambient air temperature [K]

M = Mach number [dimensionless]

γ = ratio of specific heats [dimensionless]

[1] Research Staff Member, Science & Technology Division, 4850 Mark Center Drive.
[2] Research Staff Member, Science & Technology Division, 4850 Mark Center Drive.

q'' = black body radiant flux [W/m^2]

E = illuminance (incident visible light flux) [lumens/m^2]

D = distance between reentry body and observer [m]

I_0 = luminous intensity per unit solid angle in the direction of the observer [candelas (cd)]

α = attenuation coefficient/extinction of visible light in air [m^{-1}]

α_o = attenuation coefficient/extinction of visible light in air at sea level [m^{-1}]

H = scale height of the atmosphere [m]

m = air mass traversed along line of sight from observer to reentry body [kg]

m_0 = total air mass along a vertical line from sea level to space [kg]

θ = viewing elevation angle from horizon [radians]

R_E = radius of earth [m]

z = altitude of reentry body [m]

L = apparent luminance [nits = candelas/m^2]

Ω = solid angle subtended by the light source [steradians (sr)]

Ω_{min} = minimum resolvable solid angle [steradians]

C = contrast [dimensionless]

L_o = background luminance [nits]

L/D = lift-to-drag ratio [dimensionless]

I. Introduction

Numerous videos of space shuttle and ballistic missile atmospheric reentry, freely available on the Internet, clearly demonstrate the bright optical signature presented by a hypersonic reentry body from great distances over extended periods of time. This work explores whether, when, and where a reentry body will exhibit optical signatures visible to the unaided human eye during reentry. Radiant emissions from hot gases in a shock layer that forms around the leading edge of a reentry body during its hypersonic flight through the atmosphere can generate an optical signature. We calculate variation of the signature with viewing location and time. The analysis further explores whether such signatures will be “noticeable,” a term explored herein. The paper divides the analysis into radiant emissions, optical transmission and attenuation, limits of human perception, and “noticeability.”

II. Theory

A. Radiant Emissions

When an object moves through a gas at greater than the ambient speed of sound, it generates a shockwave. As gas passes through the shockwave, its pressure, density, and temperature suddenly rise. Kinetic energy from the rapidly moving object highly energizes the gas. If the gas becomes sufficiently energetic, it will radiate electromagnetic energy with a wavelength and intensity related to its molecular content, density, and temperature Determining this spectrum of emission garnered intense interest in the early era of intercontinental ballistic missile (ICBM) development, mostly because of concerns about the resulting heat transfer to the reentry vehicle itself. Radiative heat transfer does, in fact, account for a substantial portion of the total heating of the reentry body [1]. At the high energies and temperatures associated with ICBM reentry (on the order of 7 km/s reentry velocity), molecules in the atmosphere dissociate and ionize, and the resulting emission spectrum does not resemble the classic black-body spectrum of Planck's Law. However, the emission spectrum has been characterized, and Maiden's book shows the intensity of emission in the visible spectrum from the stagnation point as a function of reentry velocity and altitude [2]. To give a sense for the scaling of the emission function, in the vicinity of 6-km/s velocity and 30-km altitude, the stagnation point radiant intensity is approximately proportional to $V^{8.5}\rho^{1.6}$, where V is the object velocity and ρ is the ambient density [3].

The temperature of the air in the shock layer diminishes as it moves along the body away from the stagnation point. The local temperature in the shock layer near a spherical nose can be characterized by the angular position away from the tip, meaning that the area of a region above a given temperature will be proportional to the square of the nose radius of curvature. The hot gases are also optically thin, meaning that the amount of radiation emitted will depend on the volume rather than the surface area. The thickness of the shock layer is proportional to the nose radius of curvature, so the volume of gas above a given temperature will scale with the cube of the nose radius of curvature. The integrated total visible spectrum radiant emission (luminous power) from the nose (accounting for the diminishing temperature away from the stagnation point) is given approximately by $\varphi = 0.1 J_S R^3_N$, where J_S is the volumetric luminous intensity at the stagnation point and R_N is the nose radius of curvature [1]. For comparison, at 6-km/s velocity and 30-km altitude, a body with a 50-cm nose radius of curvature will radiate 125 kW of visible light, about as much as 60,000 100-W incandescent bulbs (each with a visible efficiency of 2%).

Although the hot gases around the nose of a reentry body do not radiate as a black body, the black-body scaling gives a sense that one might expect strong velocity dependence. For an ideal gas with a constant specific heat (not the case at the high temperatures present in the case of interest), the stagnation temperature is proportional to the velocity squared [4],

$$T = T_\infty \frac{[2\gamma M^2-(\gamma-1)][(\gamma-1)\mathrm{M}^2+2]}{M^2(\gamma+1)^2} \underset{M\gg1}{\longrightarrow} T_\infty \frac{2\gamma(\gamma-1)}{(\gamma+1)^2} M^2 \propto V^2, \quad (1)$$

where T is the absolute stagnation temperature, T_∞ is the absolute ambient temperature, γ is the ratio of specific heats, and M is the Mach number. Black-body radiation flux, q'', described by the Stefan-Boltzmann law, $q'' = \sigma T^4$, together with the aforementioned temperature-velocity scaling, indicates that q'' is proportional to V^8.

The stagnation temperature of a real reentry body will be lower than the calorically perfect ideal gas stagnation temperature described above because, in a real gas, specific heat rises with temperature as nontranslational modes absorb energy. At very high energies, the radiation will also arise from transitions of specific molecular and ionic species present in the optically thin gas, whereas a black body produces a material-independent spectrum and behaves as an opaque surface emitter.

Ablative cooling of the reentry body may introduce smoke, soot, or other particulates into the shock layer, and these materials have the potential to render the shock layer optically thick and its radiation more like that of a black body. At the same 30-km altitude and 6-km/s velocity used previously as a reference point, the stagnation temperature is 14400 K (for a calorically imperfect but thermally perfect gas, calculated in accordance with [4]). For a spherical nose, the maximum temperature resides at the stagnation point in the front and decreases towards the nose edge. Assuming the temperature decreases by 75% at the nose edge, the temperature in this region would be 10800K [1]. The Stefan-Boltzmann Law predicts a total black-body radiant power of 600 MW, of which 30% is in the 340–540 nm band (in accordance with Planck's law) (e.g. [5]) or 180 MW versus the 125 kW predicted for the untainted hot air—a difference of 3 orders of magnitude.

B. Optical Transmission and Attenuation

Given the luminous power of the reentry body calculated using the methods of Section II.A, we next address how much of that power reaches an observer on the ground. The light radiated from the reentry body spreads, which

reduces its flux in proportion to the distance squared, and attenuates exponentially through scattering and absorption in the atmosphere according to Lambert's Law [5]. The combined effect of these two principles is known as Allard's Law [6],

$$E = \frac{I_0}{D^2} e^{-\alpha D}, \tag{2}$$

where E is the illuminance (incident visible light flux) at the observer, D is the distance separating the reentry body and observer, I_0 is the luminous intensity (the luminous power per solid angle in the direction of the observer) of the reentry body, and α is the attenuation coefficient. To evaluate the light reaching an observer, illuminance (at the observer) must be calculated. We assume that the luminous intensity is distributed omnidirectionally, so that $I_o = \varphi/(4\pi)$, where φ is the luminous power.

The attenuation coefficient at 550 nm (green light in approximately the perception-weighted center of the visible spectrum) is $\alpha_0 = 2.0 \times 10^{-5}$ m^{-1} at sea level [7]. Attenuation effectively acts per unit air mass traversed, so the attenuation along a path through the atmosphere is based on the distance at sea level required to traverse an equivalent mass of air to that along the true path. Allard's law can be expressed in terms of sea-level equivalent atmosphere traversed:

$$E = \frac{I_0}{D^2} e^{-\alpha_0 \frac{m}{m_0} H}, \tag{3}$$

where m is the air mass traversed by the line of sight between the observer and the reentry body, m_0 is the total air mass in the atmosphere along a vertical column from sea level to space, and H is the scale-height of the atmosphere over which density decreases by a factor of e (approximately 6,700 m). The amount of air in an infinitely tall column in an exponential atmosphere (An exponential atmosphere is described by $\rho = \rho_0 e^{z/H}$, where ρ is the density, ρ_0 is the density at sea level, and z is the altitude.) is equal to that in a sea-level path of length equal to the scale-height $\left(\int_0^\infty \rho dx = \rho_0 H\right)$. When viewing through the atmosphere, the viewing elevation angle, θ, has a

pronounced effect. The air mass traversed looking out beyond the atmosphere at the horizon is 38 times that looking at zenith [8]. For an exponential atmosphere, a good approximation, even near the horizon, is

$$\frac{m}{m_0} = \sqrt{\frac{\pi R_E}{2H}} e^{\frac{R_E \sin^2\theta}{2H}} \left(\operatorname{erf} \sqrt{\frac{z^2 + 2zR_E + R_E^2 \sin^2\theta}{2HR_E}} - \operatorname{erf} \frac{\sqrt{R_E} \sin\theta}{\sqrt{2H}} \right) \tag{4}$$

where R_E is the radius of the earth and z is the altitude of the object.

Equation (3) permits calculation of how much illuminance, or total visible light flux, would be incident on a ground observer. The brightness of the reentry body to the observer (i.e., the concentration of the apparent origin of the illuminance) is given by the illuminance per solid angle subtended by the reentry body from the perspective of the observer. In other words, a very bright but small source can provide as much illumination as a dim but very large source. For a resolved object without attenuation, luminance is invariant with distance because the illuminance and the solid angle subtended both diminish with the inverse square of the distance. This principle is easily observed on a long stretch of a city street that has traffic lights visible for multiple blocks ahead. Lights further and further ahead appear smaller and smaller, but the brightness of the lights appears undiminished. However, if a source is sufficiently distant that it appears as a point source (really, the minimum resolvable size), the illuminance still drops as the inverse distance squared, but the apparent size remains constant, which causes the apparent luminance to drop with the inverse distance squared. Thus, apparent luminance is given by

$$L = \frac{E}{\max(\Omega, \Omega_{\min})}, \tag{5}$$

where Ω is the solid angle subtended by the light source from the perspective of the observer, and $\Omega_{\min}$ is the minimum resolvable solid angle. Absolute luminance would be based only on the true solid angle subtended.

C. Limits of Human Perception

The most basic determinant of whether an object is discernible by the unaided human eye is its contrast with the background. Contrast, C, is defined as the excess brightness of the object relative to the background luminance, L_0:

$$C = \frac{L - L_0}{L_0}. \tag{6}$$

An object brighter than the background presents positive contrast, and an object darker than the background presents negative contrast. An object cannot have negative luminance, so contrast ranges from negative one to infinity. Path luminance (the scattering of ambient light to the observer along the viewing path) diminishes observed contrast. Path luminance, considered primarily during daytime, depends on sun elevation angle, viewing elevation angle, and viewing azimuth angle relative to the sun. Path luminance exponentially approaches background luminance in the same fashion that Lambert's law describes attenuation of object luminance [9].

The absolute value of contrast determines visibility, so negative and positive contrasts of the same magnitude contribute equally to visibility [10]. The size of an object (angle subtended) also contributes to its visibility, with larger objects being more visible. Below a critical angular size, objects appear as point sources, and size does not contribute directly to visibility. However, the absolute contrast (as opposed to apparent contrast) requirement continues to vary because the apparent luminance diverges from the absolute luminance [11]. In this regime of apparent point sources, the threshold represents a constant minimally perceptible point source illuminance.

The third variable contributing to human visibility thresholds is ambient light level. The retina—the detector in the human eye—contains two types of light sensors: rods and cones. The rods, which are far more sensitive than the cones (rods can detect a single photon), are principally used for vision in dim lighting. The cones are used for bright environments. The rods and the cones are distributed differently over the retina, and neither is distributed homogeneously. Cone-based bright-light sensitivity is principally central vision, whereas rod-based dim-light vision is highly peripheral. Because the eye adapts to the ambient light level and the dominant modes of vision vary with the adaptation to the light level, the human thresholds for discerning objects also depend on the ambient light adaptation level. Greater contrast is required at lower ambient light levels. While the human eye could discern a contrast of 0.4 in daylight, it could not discern a contrast below 710 in starlight. The critical angular size below which objects appear as point sources also grows with lower ambient light levels, ranging, for example, from 0.2 mrad in daylight to 2 mrad in starlight. Blackwell quantified the threshold contrast level as a function of object size and ambient light level [11].

D. Noticeability

Blackwell based his results for contrast thresholds on experiments conducted to discover the bare minimum required for 50% probability of discernment of an object in a known position and with a long observation period [11]. In this study, we are concerned not just with visibility, but also with what might be termed "noticeability." The question is not what might be barely discerned with careful study of a prespecified location but rather what a casual observer would notice without cueing or foreknowledge and without necessarily looking in exactly the right place at the right time.

Many studies have been conducted on what is termed "attention capture," (i.e., what people will notice). Relevant here, in particular, are two terms: "reflexive" attention capture, meaning that the subject's attention is involuntarily drawn, and "explicit" attention capture, meaning that the subject is aware that his/her attention has been captured. (There is also implicit or subconscious attention capture in which a subject is distracted from a primary task by the appearance or presence of the target object even though his/her focus does not shift to it.) The results have shown significant variation depending upon the task in which subjects were engaged, state of mind of the subjects, dynamics of the target object (moving versus stationary), colors, uniformity or pattern of the background, presence of other objects competing for attention, distance of the target object from the center of fixation (where the subject was looking), expectations of the subject regarding the appearance or presence of the object, and so forth. In other words, the variables are too numerous to extrapolate a single generic explicit reflexive attention capture threshold [12].

Instead of deriving a theoretical threshold, we use an analogous situation to provide a meaningful metric for the evaluation of noticeability. The Federal Aviation Administration (FAA) has established regulations for the installation of obstruction lighting on tall structures to alert pilots of their presence and avoid collisions. In other words, the FAA has established a standard for a particular type of explicit reflexive attention capture device to ensure that pilots, unaware of the presence or location of such a beacon in advance, notice and attend to beacons within their fields of view. For example, for white non-strobe lights, the FAA mandates obstruction lights of 100,000 candela luminous intensity to provide daytime visibility (noticeability) at 4.3 km on a day with 4.8-km meteorological visibility[3] [13]. From Allard's Law, the illuminance under these conditions is 3.6×10^{-4} lumens/m^2.

[3] Standardized visibility distance is calculated from the atmospheric attenuation coefficient (α). For daytime conditions, $\alpha = 3/\text{visibility}$. For nighttime conditions, $\alpha = -\ln(\text{visibility}/4.79 \times 10^5 \text{ m})/\text{visibility}$ [17]. Another possibility is the Koschmieder Equation, $\alpha = 3.912/\text{visibility}$, which fits better with the data in the FAA bulletin [9].

For the hazy conditions that give rise to this visibility level, we presume the background brightness to be equivalent to an overcast sky, approximately 300 cd/m^2 [14]. The critical visual angle at that adaptation brightness is approximately 0.2 mrad (3×10^{-8} sr) [11], so at 4.3-km distance, any source smaller than 90 cm would appear as a point source. For a source falling into that regime, the apparent brightness of the obstruction lighting (in addition to the superimposed background and path luminance) would be 12,000 cd/m^2, and the contrast would be 39 compared to a threshold of 0.37 for a ratio of approximately 100. The same can be done for the nighttime requirements to yield a contrast ratio of 200–400, depending on the method of inference of the attenuation coefficient from reported visibility. In both cases, the FAA lighting requirement is on the order of a few hundred times the minimum contrast threshold for detectability. For this study, we take the 400x threshold contrast level as the standard for high noticeability.

III. Results

In Fig. 1, we show four manners of characterizing the visual signature of a reentry body at an instant in time. For this example, we use a reentry body with a nose/leading-edge radius of curvature of 0.5 m, a velocity of 7 km/s, and an altitude of 50 km. Figure 1a (top left) shows the preferred metric, which will be used in what follows. Our preferred metric is the contrast level normalized to the threshold contrast level. A value of 1 indicates marginal detectability, and a value of 400 indicates noticeability equivalent to FAA standards for obstruction lights. Both of these levels are indicated on the plot. The value of the metric is then plotted as a function of the ground distance of an observer from nadir below the reentry body. Curves are shown for four different ambient light adaptation levels: dark cloudless (moonless) night (labeled 'Star'), full moon night (labeled 'Moon'), zenith brightness at sunset (labeled 'Twilight'), and zenith brightness at 10:30 A.M (labeled 'Day').[4]

Figure 1a shows that the given reentry body would be noticeable at night at distances of nearly 500 km from nadir, even on a full moon night; however, during the day, it would be detectable but not noticeable to the 400x threshold standard, even from directly below. Figure 1b shows the raw, unnormalized contrast level. Figure 1c shows the amount of light cast by the reentry body on the ground in the form of illuminance or flux of visible light power. Figure 1d shows astronomical apparent magnitude (V-band), which is a measure astronomers use to rate the visibility of celestial bodies. Apparent magnitude measures relative illuminance and is really designed for point

[4] Representing a sun elevation angle of 60°, corresponding to 10:30 A.M. in Washington, D.C., on July 21, 2009.

sources. The scale is logarithmic (with lower magnitude meaning brighter) and five steps in magnitude corresponding to a factor of 100 in illuminance [15]. The full moon has an average magnitude of -12.7, and Venus has an average magnitude of -4.4 [16]. For those familiar with magnitudes, Fig. 1d allows ready comparison of reentry body appearance with known celestial objects. Venus, for instance, is highly visible at night but only marginally visible during the day. Only the threshold-normalized contrast ratio from Fig. 1a will be used in what follows.

We now consider four cases of reentry bodies, varying their lift-to-drag ratios L/D and their initial flight path angles. For each case, the reentry body, with a nose radius of curvature of 0.5 m, a drag coefficient of 0.3, a diameter of 1 m, and a mass of 1000 kg, begins at an altitude of 150 km with a velocity of 7 km/s. For the first case, we consider a purely ballistic trajectory with L/D = 0 and an initial flight path angle of -26°. For the following three cases, we consider L/D = 0.3 with an initial flight path angle of -10°, L/D = 0.5 with an initial flight path angle of -5°, and L/D = 2 with an initial flight path angle of -2°. In Figs. 2 to 17 we show trajectories, noticeability regions and durations, and elapsed time from first noticeability to impact.

IV. Conclusion

For a given reentry body, methods in this paper allow calculation of noticeability and visibility regions with a reasonably simple criterion for assessing noticeability by analogy to FAA lighting visibility requirements. For many conditions, particularly at night, reentry bodies may be noticeable for hundreds of kilometers around the impact point for periods of time ranging from tens of seconds to minutes before impact. Purely ballistic reentry bodies of the scale in the examples shown would be noticeable for hundreds of kilometers at night over regions including the impact point but for less than a minute prior to impact. Strongly lifting reentry bodies could be visible thousands of kilometers and tens of minutes in advance of the impact site as they skip off the denser atmosphere, but they would slow sufficiently with successive skips that, by the time they come over the impact point's horizon, they would no longer be noticeable.

Appendix

A derivation of the air mass approximation is given here. The law of cosines relates viewing elevation angle, range, and altitude. For any point along the line of sight,

$$(z + R_E)^2 = R_E^2 + x^2 - R_E x \cos\left(\theta + \frac{\pi}{2}\right), \tag{A1}$$

where x is the distance from the observer of a point along the line of sight and z is the altitude of that point. This relationship can be solved for x or z:

$$z = \sqrt{x^2 + 2xR_E \sin\theta + R_E^2} - R_E \tag{A2}$$

or

$$x = \sqrt{z^2 + 2zR_E + R_E^2 \sin^2\theta} - R_E \sin\theta. \tag{A3}$$

The mass of air traversed relative to m_0 is

$$\frac{m}{m_0} = \frac{1}{\rho_0 H}\int_0^x \rho_0 e^{-\frac{z}{H}} dx = \frac{1}{H}\int_0^x e^{-\frac{\sqrt{x^2+2xR_E\sin\theta+R_E^2}-R_E}{H}} dx\,. \tag{A4}$$

For $x \ll R_E$, Eq. (A2) can be approximated by the first two terms of a Taylor series expansion of the radical about R_E

$$z \approx \frac{1}{2}\frac{x^2}{R_E} + x\sin\theta, \tag{A5}$$

and Eq. (A4) can in turn be approximated by

$$\frac{m}{m_0} = \frac{1}{H}\int_0^x e^{-\frac{\frac{1}{2}x^2 + xR_E\sin\theta}{HR_E}} dx\,. \tag{A6}$$

Equation (A6) can be evaluated by completing the square in the exponent,

$$\frac{m}{m_0} = \frac{1}{H} e^{\frac{1R_E}{2\,H}\sin^2\theta} \int_0^x e^{-\frac{(x+R_E\sin\theta)^2}{2HR_E}} dx \; = \sqrt{\frac{\pi R_E}{2H}} e^{\frac{1R_E}{2\,H}\sin^2\theta} \left(\operatorname{erf} \frac{D+R_E\sin\theta}{\sqrt{2HR_E}} - \operatorname{erf} \frac{R_E\sin\theta}{\sqrt{2HR_E}} \right). \tag{A7}$$

Recasting Eq. (A7) in terms of the altitude of the reentry body instead of the distance to it along the line of sight,

$$\frac{m}{m_0} = \sqrt{\frac{\pi R_E}{2H}} e^{\frac{R_E\sin^2\theta}{2H}} \left(\operatorname{erf} \sqrt{\frac{z^2+2zR_E+R_E^2\sin^2\theta}{2HR_E}} - \operatorname{erf} \frac{\sqrt{R_E}\sin\theta}{\sqrt{2H}} \right). \tag{A8}$$

The accuracy of Eq. (A8) can be bounded by bounding the error in Eq. (A5). Using the exact relationship, Eq. (A3), let us evaluate the ratio of the approximate altitude to the true altitude,

$$\frac{\frac{1x^2}{2R_E}+x\sin\theta}{z} = \frac{z}{2R_E} + 1. \tag{A9}$$

Using the approximation therefore amounts to underestimating the true local density (by overestimating the altitude) with an estimate that gets worse with increasing altitude. Comparing the approximation of Eq. (A8) for an object at 150 km altitude to the tabulated data in Young [8] shows that the error does not exceed 0.15% for elevation angles above 2 degrees and peaks at 1.8% error for a horizontal path.

References

[1] Martin, J.J., *Atmospheric Reentry*, Prentice-Hall, Englewood Cliffs, NJ, 1966.

[2] Maiden, C. J., "Aerophysical Studies at Hypersonic Velocities in Free Flight Ranges," *Advances in Aeronautical Sciences: Proceedings of the second International Congress in the Aeronautical Sciences*, Vol. 4, Pergamon Press, Oxford, 1962, pp. 675-699.

[3] Hidalgo, H. and Detra, R. W., "Generalized Heat Transfer Formulas and Graphs for Nose Cone Reentry into the Atmosphere," *Journal of the American Rocket Society*, Vol. 31, No. 3, 1961, p. 318.

[4] Ames Research Staff, "Equations, Tables, and Charts for Compressible Flow," National Advisory Committee for Aeronautics Report 1135, 1953.

[5] Mills, A. F., *Heat and Mass Transfer*, Richard D. Irwin, Inc., Boston, 1995, p. 547.

[6] Brown, E. B., *Modern Optics*, Reinhold Publishing Corp., New York, 1965.

[7] Miller, J. L. and Friedman, E., *Photonics rules of thumb: optics, electro-optics, fiber optics, and lasers*, McGraw-Hill, New York, 1996.

[8] Scolnik, R. and Dunkelman, L., "Solar Spectral Irradiance and Vertical Atmospheric Attenuation in the Visible and Ultraviolet," *Journal of the Optical Society of America*, Vol. 49, No. 4, 1959, pp. 356-367.

[9] Young, A. T. and Kasten, F., "Revised optical air mass tables and approximation formula," *Applied Optics*, Vol. 28, No. 22, 1989, pp. 4735-4738.

[10] Koschmieder, H., "The theory of horizontal visual range," NASA TT F-14,930, June 1973, translated from "Theorie der horizontalen Sichtweite," *Beitrage zur physik der freien Atmosphäre*, Vol. 12, 1924, pp. 33-55.

[11] Gordon, J., "Visibility: Optical Properties of Objects and Backgrounds," *Applied Optics*, Vol. 3, No. 5, 1964, pp. 556-562.

[12] Blackwell, H. R., "Contrast Thresholds of the Human Eye," *Journal of the Optical Society of America*, Vol. 36, No. 11, 1946, pp. 624-643.

[13] Most, S. B. and Simons, D. J., "Attention Capture, Orienting, and Awareness," *Attraction, Distraction, and Action: Multiple Perspectives on Attentional Capture*, edited by C. L. Folk and B. S. Gibson, Advances in Psychology Vol. 133, Elsevier Science B.V., Amsterdam, 2001, pp. 151-173.

[14] U.S. Department of Transportation, Federal Aviation Administration, "Obstruction Marking and Lighting," *Advisory Circular AC 70/7460-1K*, February 2007, Appendix 2.

[15] Crawford, D. L., "Photometry: Terminology and Units in the Lighting and Astronomical Sciences," *The Observatory*, Vol. 117, 1997, pp. 14-18.

[16] Zombeck, M., *Handbook of Space Astronomy and Astrophysics*, Cambridge University Press, Cambridge, UK, 1990.

[17] Ridpath, I. (ed.), *Norton's 2000.0 Star Atlas and Reference Handbook*, 18th ed., Longman Scientific and Technical, Essex, 1989.

[18] Dixon, M., Rasmussen, R. and Landolt, S., "Short-Term Forecasting of Airport Surface Visibility Using Radar and ASOS," *11th conference on aviation, range, and aerospace*, 10.6, Hyannis, MA. 2004.

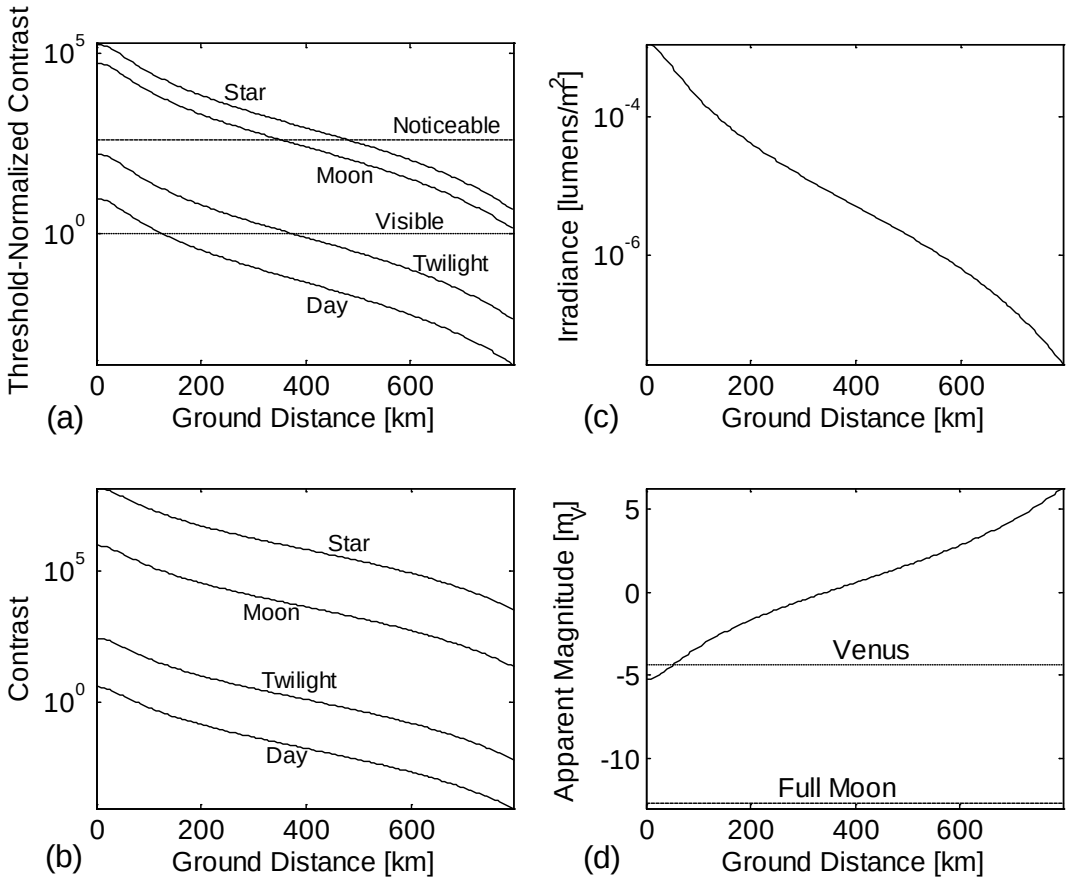

Fig. 1 Metrics for visibility: (a) normalized contrast, (b) contrast, (c) illuminance, (d) astronomical apparent magnitude (V-band). In (a) and (b), the curves are labeled according to the background. 'Day' indicates zenith at 10:30 A.M. 'Twilight' indicates zenith at sunset. 'Moon' indicates the night sky during a full moon. Star indicates a dark starlit night. In (a), the thresholds for visibility and noticeability are indicated. In (d), the apparent magnitude of Venus and the full moon are indicated.

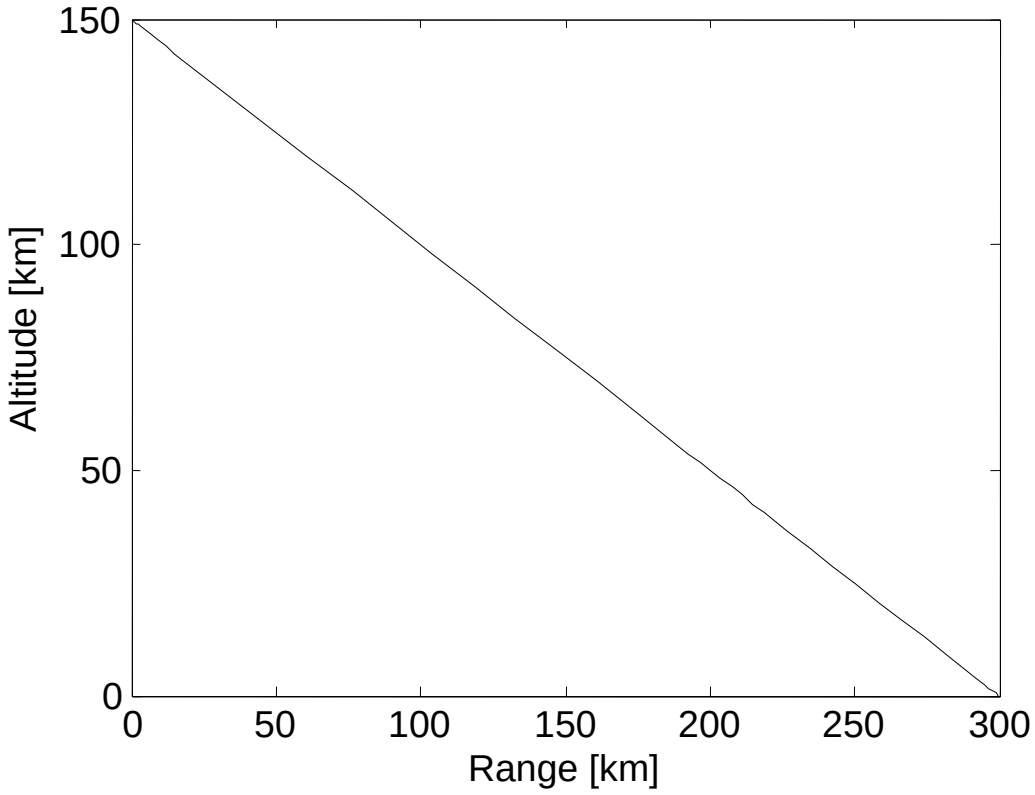

Fig. 2 Reentry trajectory, L/D=0 (pure ballistic)

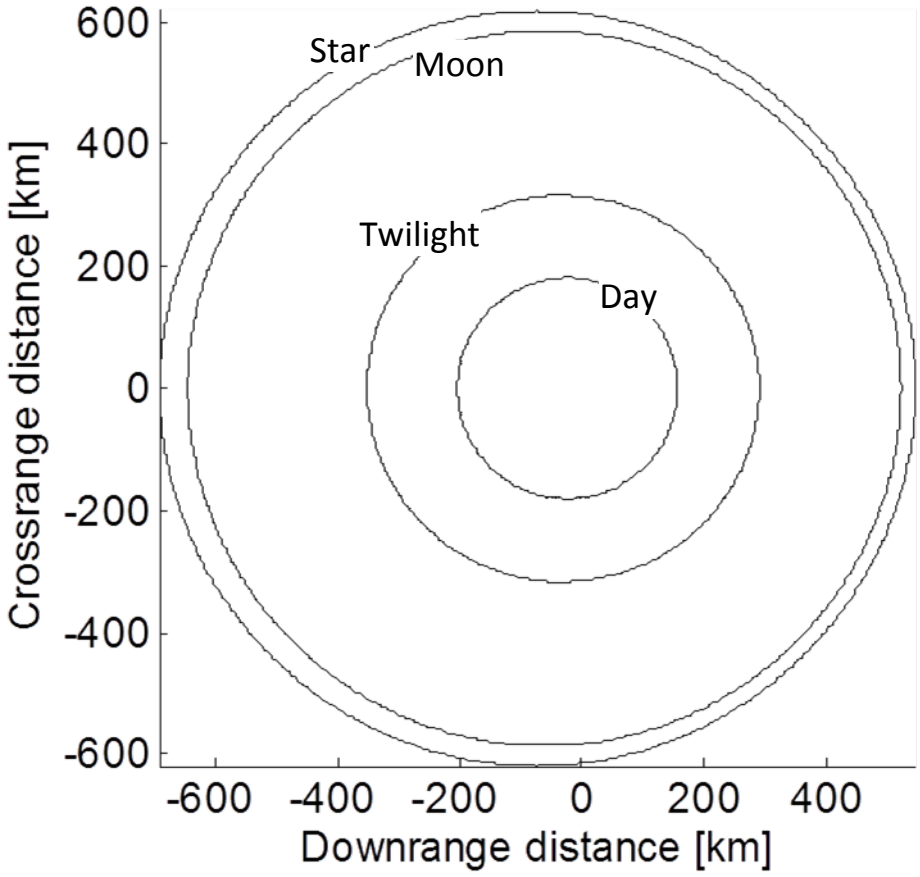

Fig. 3 Noticeability regions, L/D = 0. The contour labels refer to the sky background conditions. 'Day' indicates zenith at 10:30 A.M. 'Twilight' indicates zenith at sunset. 'Moon' indicates the night sky during a full moon. 'Star' indicates a dark starlit night. We use this convention for all the cases to follow.

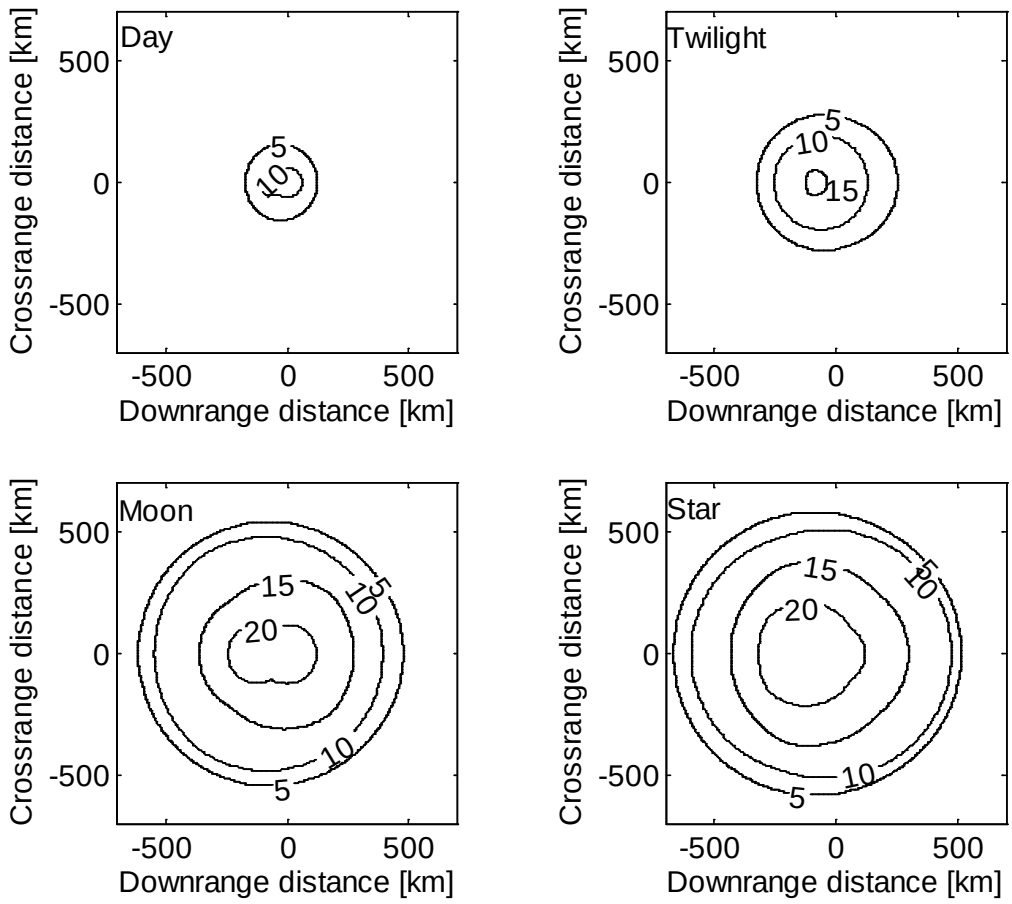

Fig. 4 Duration of noticeability [seconds], L/D = 0

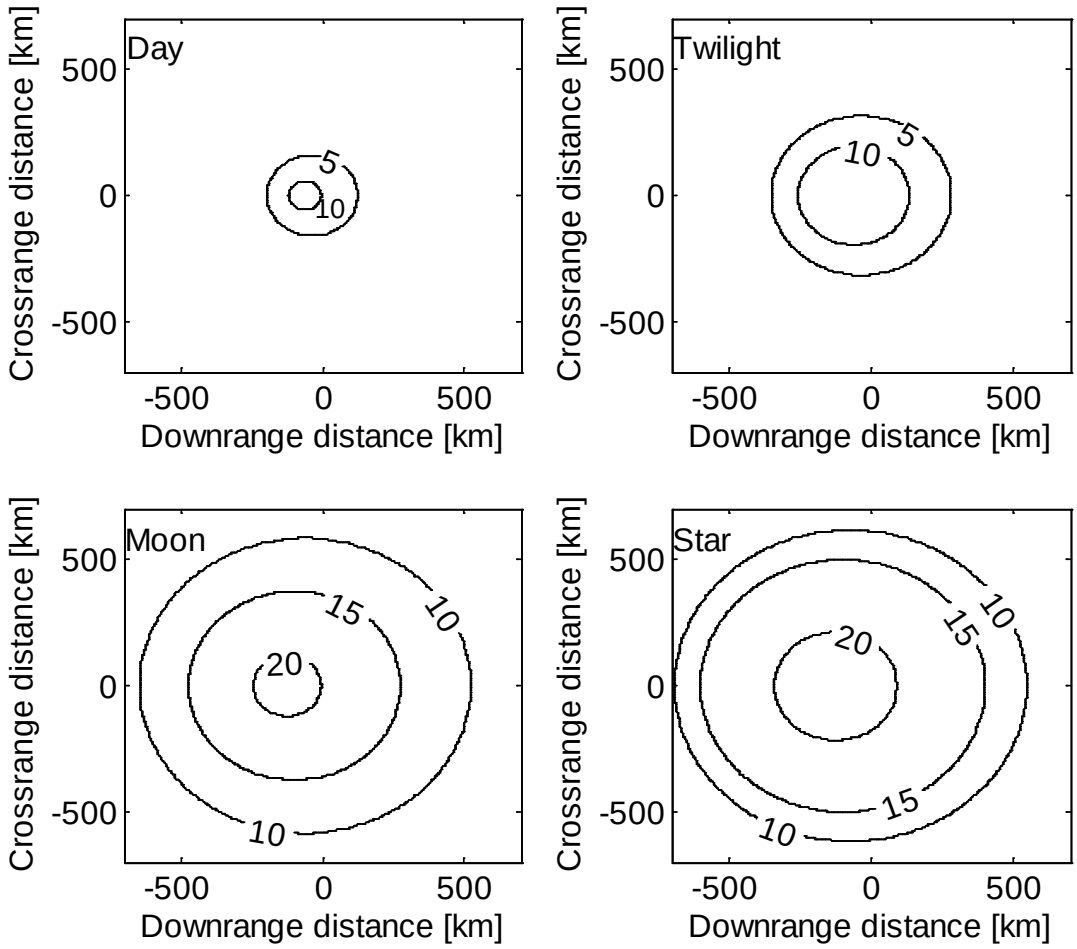

Fig. 5 Time elapsed from first noticeability to impact [seconds], L/D = 0

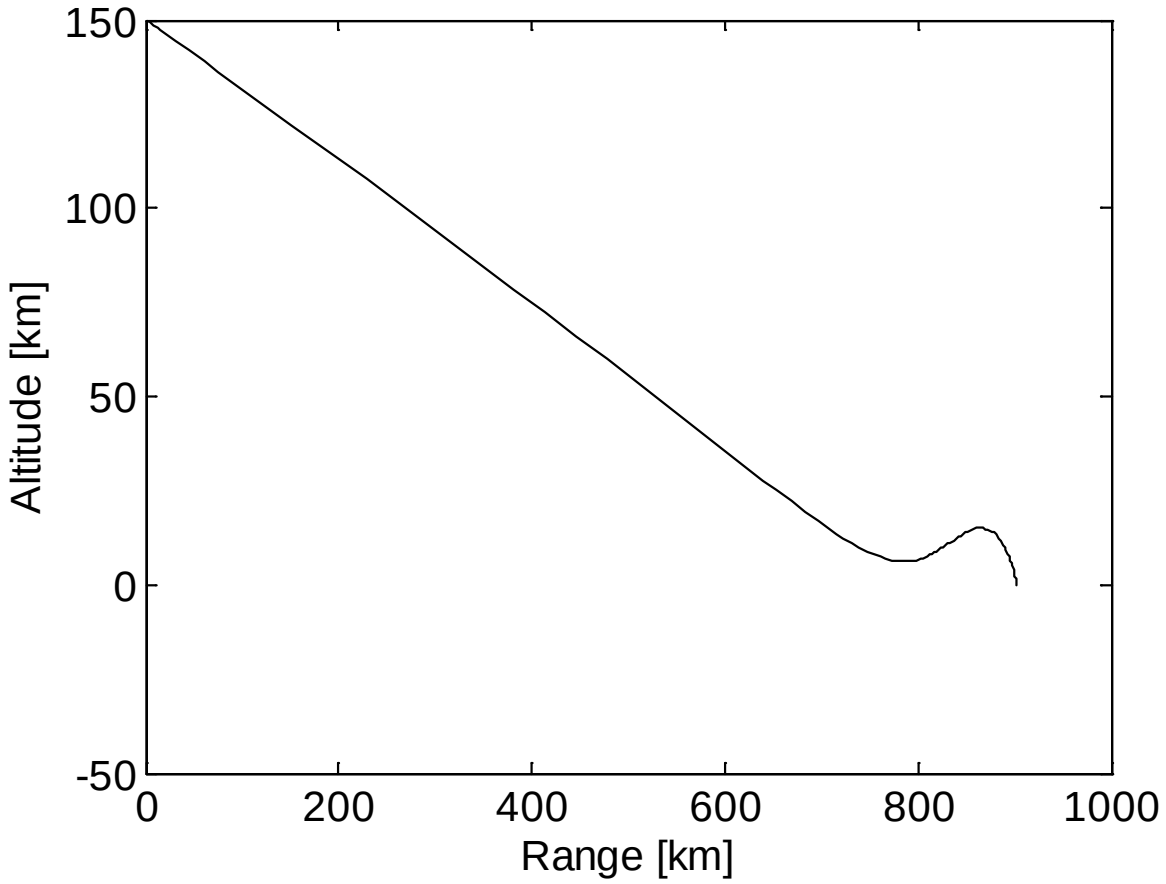

Fig. 6 Reentry trajectory, L/D = 0.3

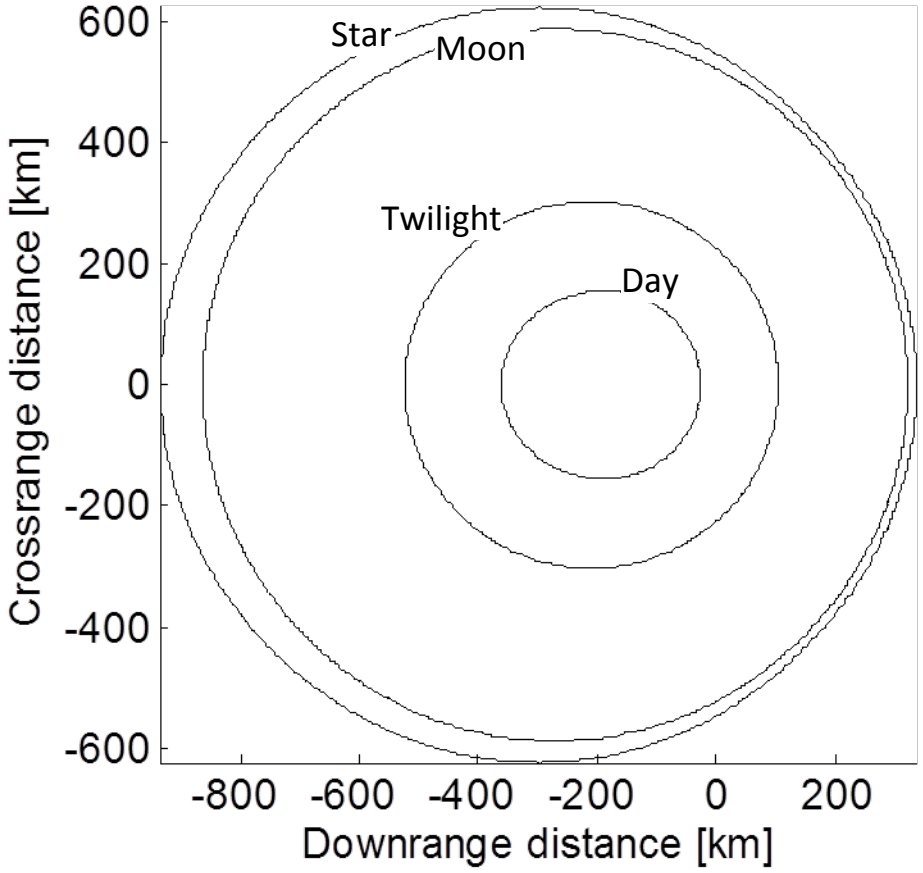

Fig. 7 Noticeability regions, L/D = 0.3

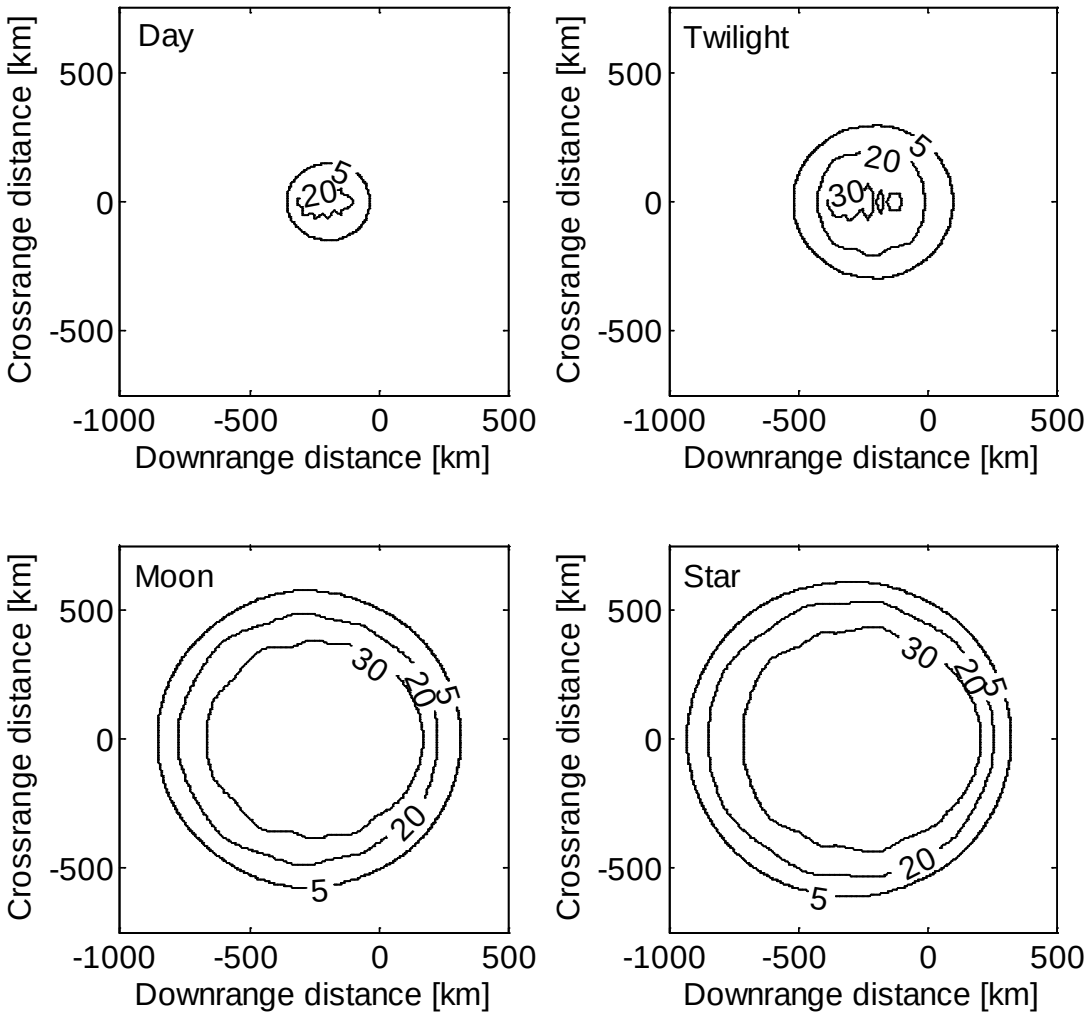

Fig. 8 Duration of noticeability [seconds], L/D = 0.3

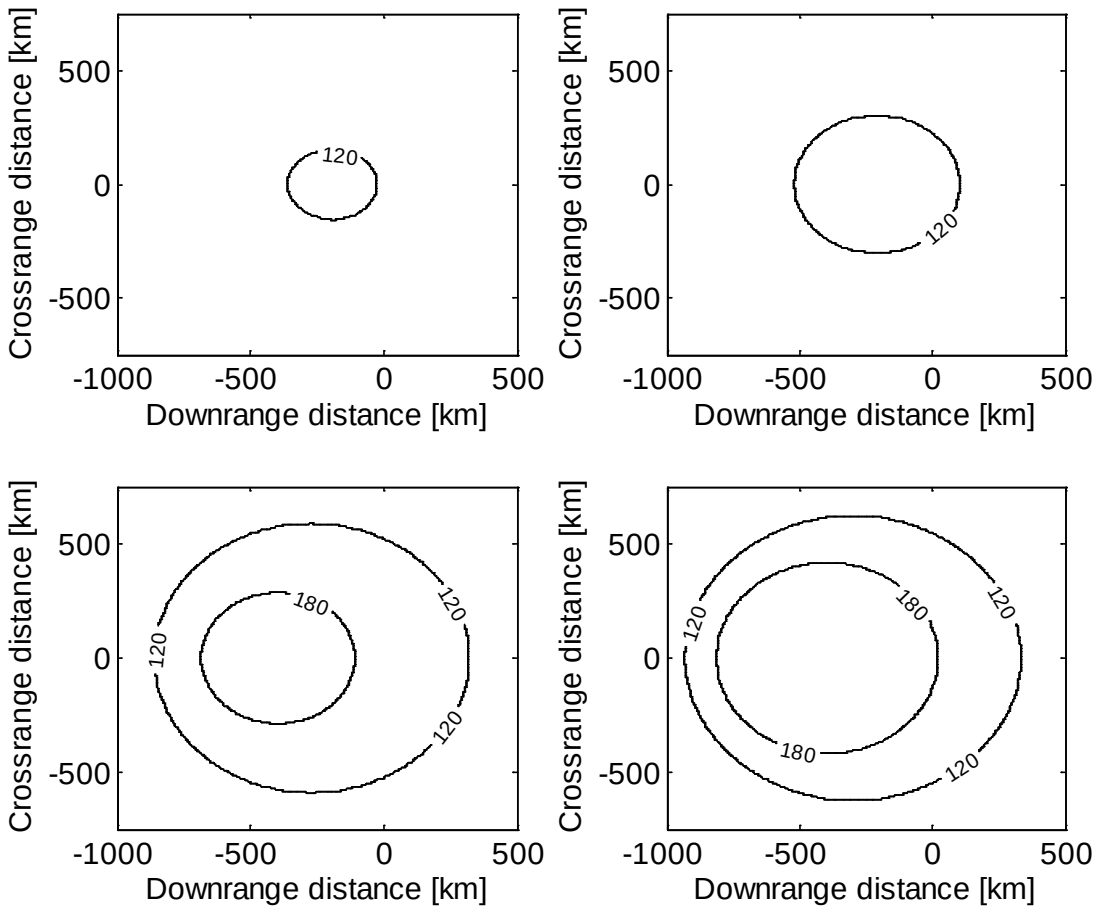

Fig. 9 Time elapsed from first noticeability to impact [seconds], L/D = 0.3

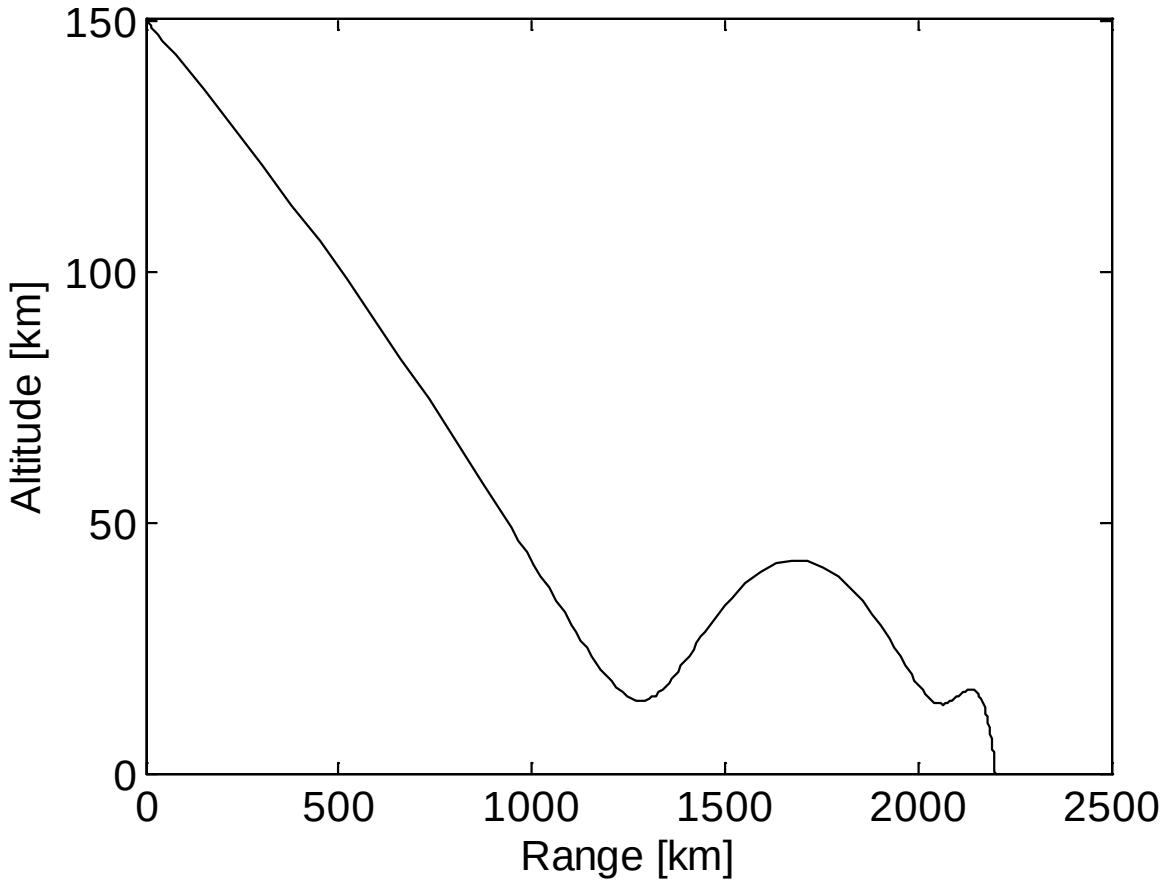

Fig. 10 Reentry trajectory, L/D = 0.5

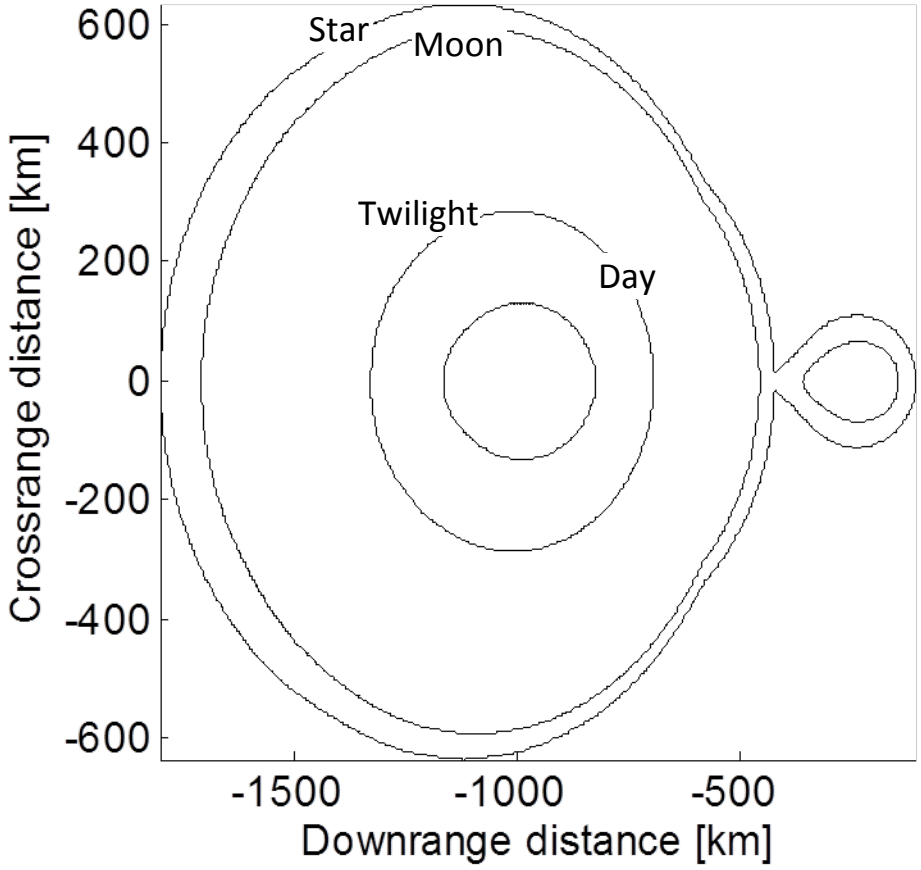

Fig. 11 Noticeability regions, L/D = 0.5

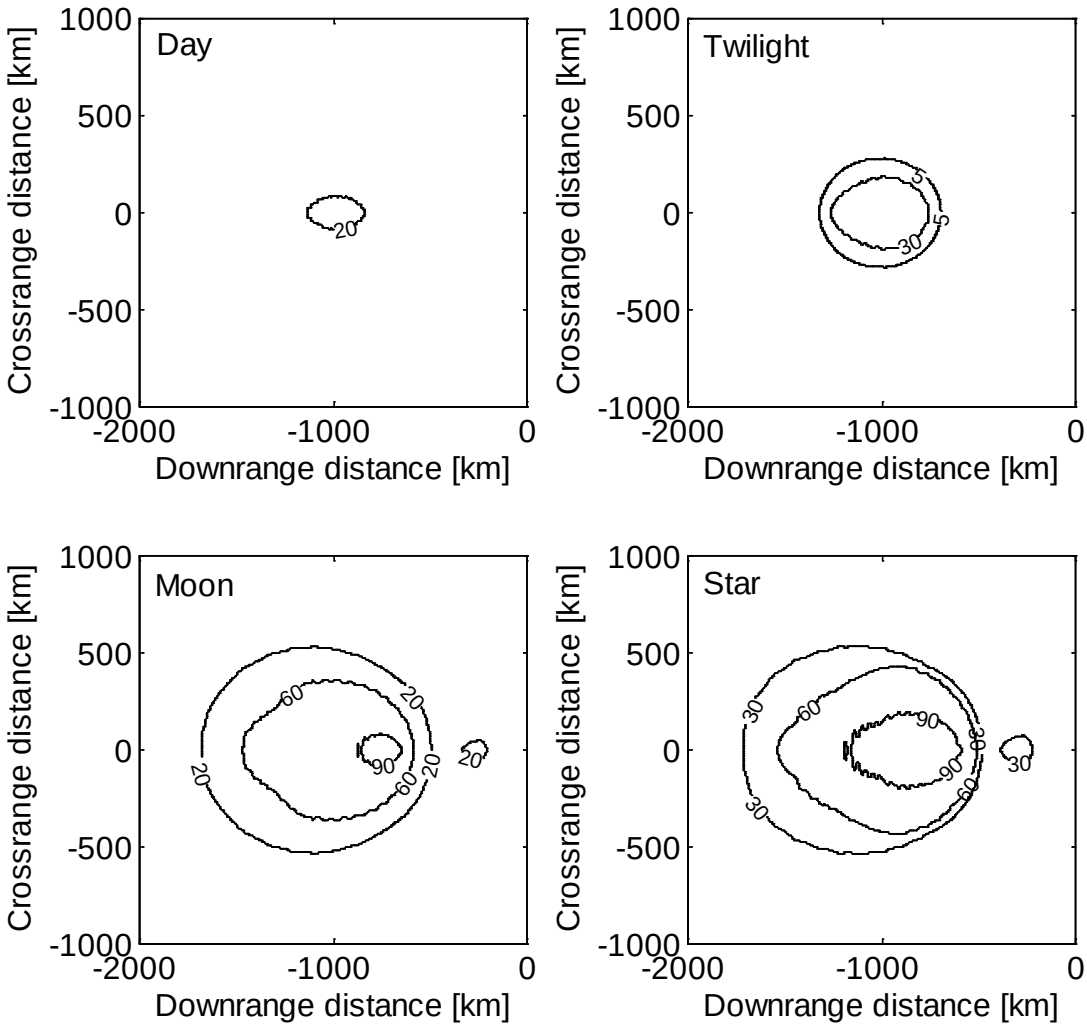

Fig. 12 Duration of noticeability [seconds], L/D = 0.5

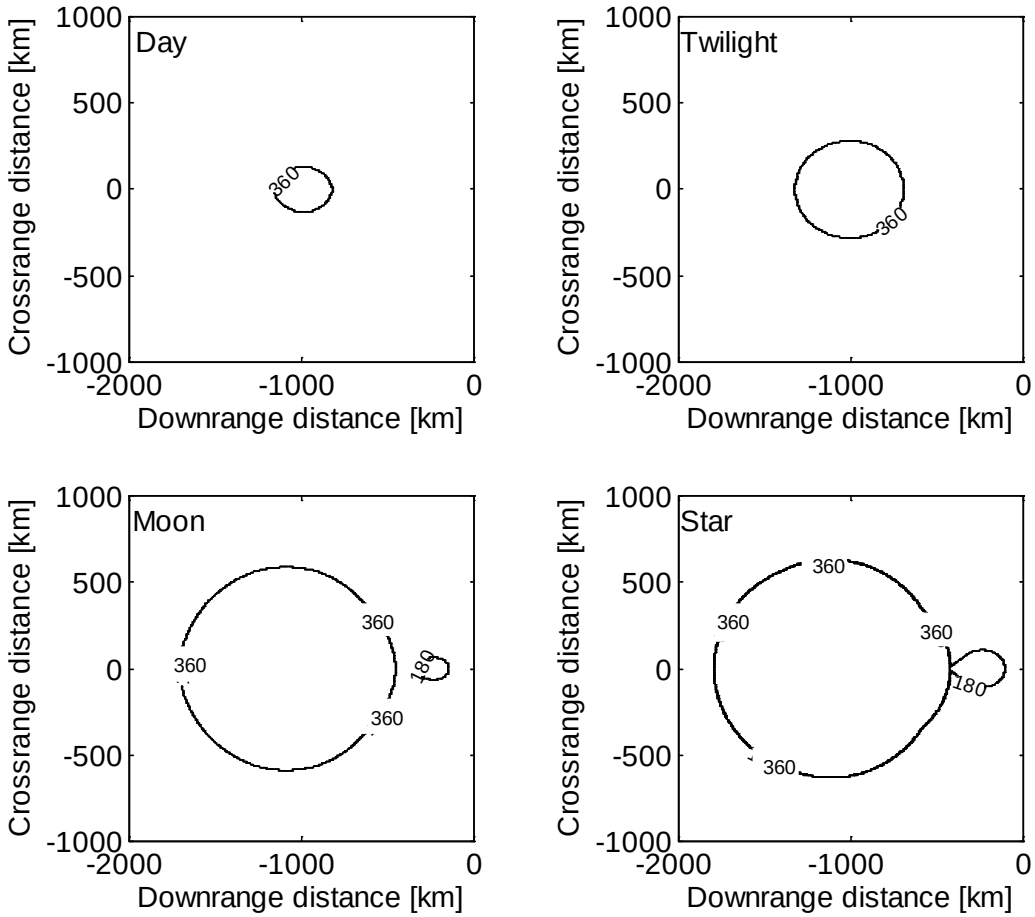

Fig. 13 Time elapsed from first noticeability to impact [seconds], L/D = 0.5

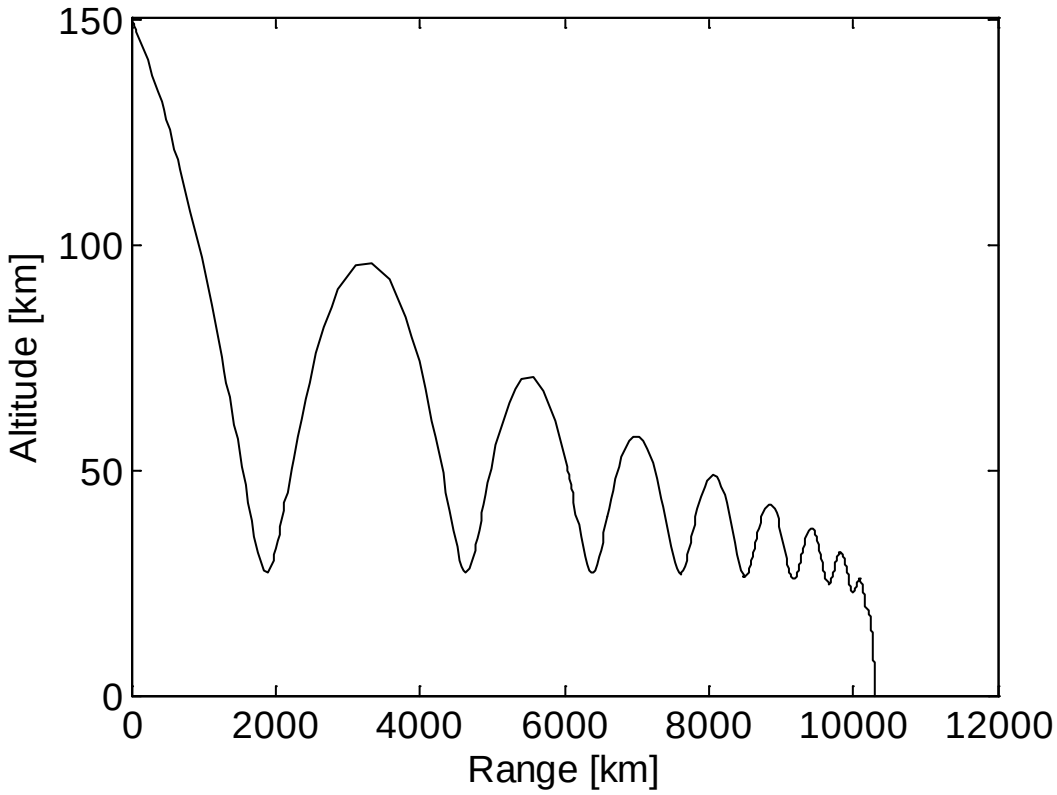

Fig. 14 Reentry trajectory, L/D = 2

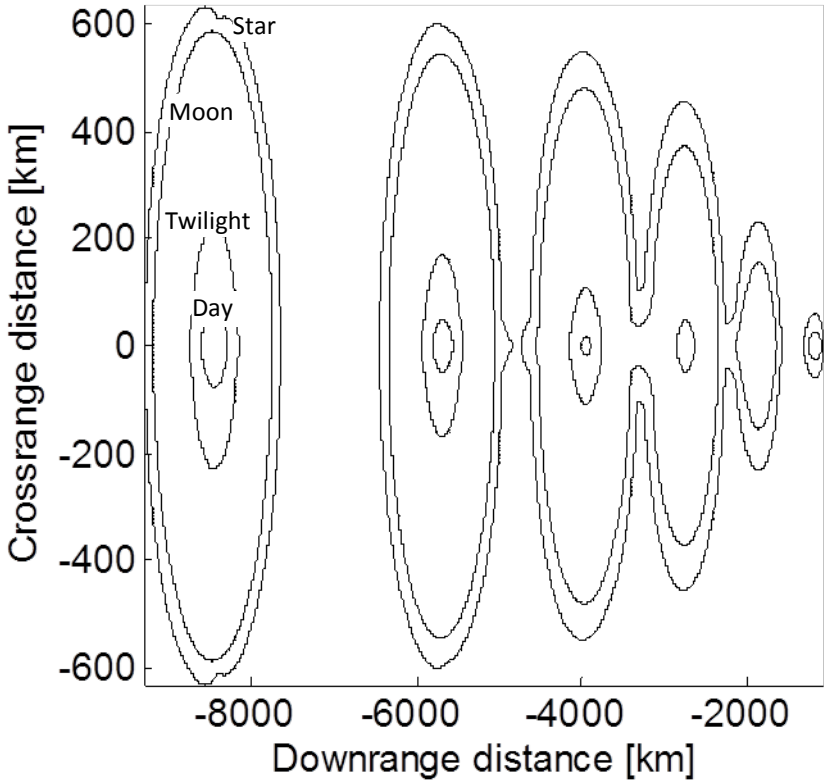

Fig. 15 Noticeability regions, L/D = 2

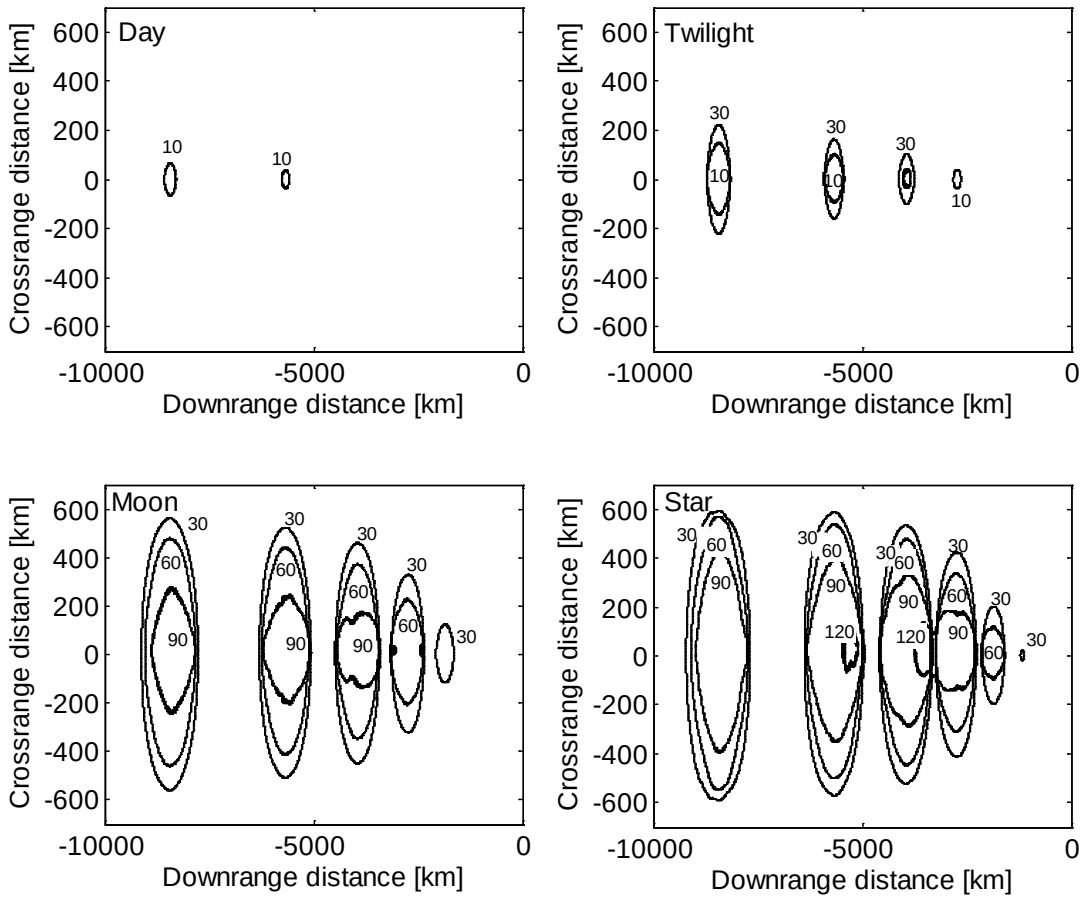

Fig. 16 Duration of noticeability [seconds], L/D = 2

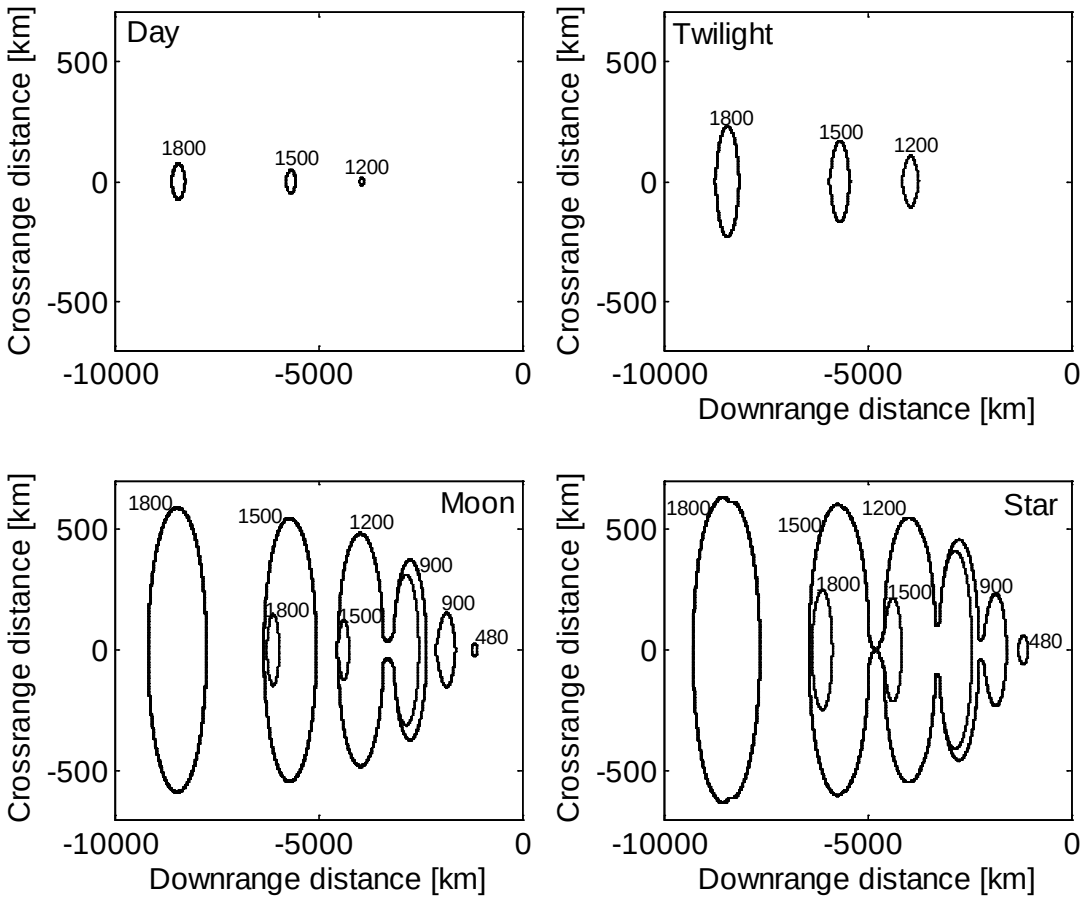

Fig. 17 Time elapsed from first noticeability to impact [seconds], L/D = 2

REPORT DOCUMENTATION PAGE

Form Approved
OMB No. 0704-0188

1. REPORT DATE	2. REPORT TYPE	3. DATES COVERED *(From–To)*
February 2013	Final	June 2012 – February 2013

4. TITLE AND SUBTITLE

Visible Signatures of Hypersonic Reentry

5a. CONTRACT NUMBER
W91WAW-09-C-0003

5b. GRANT NUMBER

5c. PROGRAM ELEMENT NUMBER

6. AUTHOR(S)

Jeremy Teichman
Leon Hirsch

5d. PROJECT NUMBER

5e. TASK NUMBER
CRP 2165

5f. WORK UNIT NUMBER

7. PERFORMING ORGANIZATION NAME(S) AND ADDRESS(ES)

Institute for Defense Analyses
4850 Mark Center Drive
Alexandria, VA 22311-1882

8. PERFORMING ORGANIZATION REPORT NUMBER

IDA Document NS D-4792
Log: H13-000192

9. SPONSORING/MONITORING AGENCY NAME(S) AND ADDRESS(ES)

Institute for Defense Analyses
4850 Mark Center Drive
Alexandria, VA 22311-1882

10. SPONSOR/MONITOR'S ACRONYM(S)

11. SPONSOR/MONITOR'S REPORT NUMBER(S)

12. DISTRIBUTION/AVAILABILITY STATEMENT

Approved for public release; distribution is unlimited. (13 March 2013)

13. SUPPLEMENTARY NOTES

14. ABSTRACT

Aerothermal heating of hypersonic reentry bodies can generate significant radiation of visible light. Here, we investigate the conditions for ground-level visibility and what we term noticeability of that radiated light to the unaided human eye. We consider radiated visible light, transmission to ground level as a function of relative observer position, sky background contrast, human contrast perception limits, and psychophysical considerations for attention capture. Considering both pure ballistic trajectories and lifting-body trajectories, we show some examples where we calculate the spatial and temporal viewing zones for both detectability and noticeability. In some cases, these viewing zones extend a significant distance from the impact location and/or include the impact location for a potentially significant period of time before impact.

15. SUBJECT TERMS

16. SECURITY CLASSIFICATION OF:			17. LIMITATION OF ABSTRACT	18. NUMBER OF PAGES	19a. NAME OF RESPONSIBLE PERSON
					Mr. Philip Major
a. REPORT Uncl.	b. ABSTRACT Uncl.	c. THIS PAGE Uncl.	SAR	34	19b. TELEPHONE NUMBER *(include area code)* 703-845-2201

Standard Form 298 (Rev. 8-98)
Prescribed by ANSI Std. Z39.18